Future precipitation projections over central and southern Africa and the adjacent Indian Ocean: what causes the changes and the uncertainty?

Article (Published Version)

Future Precipitation Projections over Central and Southern Africa and the Adjacent Indian Ocean: What Causes the Changes and the Uncertainty?

MELISSA J. LAZENBY AND MARTIN C. TODD

Department of Geography, University of Sussex, Brighton, United Kingdom

ROBIN CHADWICK

Met Office Hadley Centre, Exeter, United Kingdom

YI WANG

Department of Geography, University of Sussex, Brighton, United Kingdom

(Manuscript received 12 May 2017, in final form 5 March 2018)

ABSTRACT

Future projections of precipitation at regional scales are vital to inform climate change adaptation activities. Therefore, is it important to quantify projected changes and associated uncertainty, and understand model processes responsible. This paper addresses these challenges for southern Africa and the adjacent Indian Ocean focusing on the local wet season. Precipitation projections for the end of the twenty-first century indicate a pronounced dipole pattern in the CMIP5 multimodel mean. The dipole indicates future wetting (drying) to the north (south) of the climatological axis of maximum rainfall, implying a northward shift of the ITCZ and south Indian Ocean convergence zone that is not consistent with a simple ''wet get wetter'' pattern. This pattern is most pronounced in early austral summer, suggesting a later and shorter wet season over much of southern Africa. Using a decomposition method we determine physical mechanisms underlying this dipole pattern of projected change, and the associated intermodel uncertainty. The projected dipole pattern is largely associated with the dynamical component of change indicative of shifts in the location of convection. Over the Indian Ocean, this apparent northward shift in the ITCZ may reflect the response to changes in the north–south SST gradient over the Indian Ocean, consistent with a ''warmest get wetter'' mechanism. Over land subtropical drying is relatively robust, particularly in the early wet season. This has contributions from dynamical shifts in the location of convection, which may be related to regional SST structures in the southern Indian Ocean, and the thermodynamic decline in relative humidity. Implications for understanding and potentially constraining uncertainty in projections are discussed.

1. Introduction

Africa is highly vulnerable to climate change, evident from the reliance on seasonal precipitation for agriculture, water supply, and energy generation over the majority of sub-Saharan Africa (Basher and Briceño 2006; Meadows 2006). The region exhibits relatively low adaptive capacity (Kusangaya et al. 2014), as the El Niño drought event of 2015/16 amply demonstrates (Archer et al. 2017; Baudoin et al. 2017). Therefore, future changes in rainfall over this region need to be identified and understood, such that stakeholders, from civil society to policymakers, can make informed decisions about future adaptation planning in key sectors (Collins et al. 2012; Knutti et al. 2010).

Denotes content that is immediately available upon publication as open access.

Supplemental information related to this paper is available at the Journals Online website: https://doi.org/10.1175/JCLI-D-17-0311.s1.

Corresponding author: Melissa J. Lazenby, m.lazenby@sussex.ac.uk

DOI: 10.1175/JCLI-D-17-0311.1

We focus here on southern Africa, where the rainfall climate (see Figs. S1 and S2 in the online supplemental material) is broadly characterized by a local summer wet season in austral summer, a pronounced rainfall gradient from the dry southwest to the humid north and northeast, and a peak wet season rainfall maximum extending from the continent into the adjacent southwest Indian Ocean, referred to as the south Indian Ocean convergence zone (SIOCZ; e.g., Lazenby et al. 2016), a preferred locus for tropical–temperate weather systems. For this region the multimodel mean projections from the CMIP3 and CMIP5 model ensembles show a degree of consistency in the dominant signals of change with drier austral summer conditions projected over the southwest of the region as well as a northeasterly shift in the SIOCZ and a later onset of the rainy seasons with indications of early cessation of rainfall (Niang et al. 2014; Shongwe et al. 2009).

For most of the tropics, at least at regional scales relevant to decision-making, considerable uncertainty is evident across the ensemble of global and regional models currently available in both sign and magnitude of future precipitation projections (Rowell 2012; Knutti and Sedláček 2013; McSweeney and Jones 2013). Central and southern Africa are no exception (see section 3) and there is a clear need for improved understanding due in part to a complex climatological setting in which regional climate drivers as well as remote influences affect the region (Christensen et al. 2013; IPCC 2007; Kusangaya et al. 2014). This presents challenges to climate adaptation policy, and the persistence of uncertainty in climate projections has led to the development of "decision-making under climate uncertainty" approaches in adaptation (e.g., Hallegatte et al. 2012). These approaches appreciate the cascade of uncertainty typically associated with climate risk assessment, resulting from climate projections, downscaling techniques, impact modeling, and so on, and emphasize appropriate methods for managing risk under such conditions including, for example, robust or low regrets options or adaptive management (e.g., Dessai et al. 2009).

There is therefore considerable interest in improving our understanding of physical mechanisms driving the particular patterns of projected model changes, so that we may determine and potentially improve the robustness and credibility of projections. The physical processes driving projected change are numerous and may vary among models. Projection uncertainty is a result of varying processes found within models including, among others, parameterization schemes, climate sensitivity, and regional patterns of SST changes.

Based on analyses of projections, various mechanisms have been proposed that link increased global temperatures and precipitation changes, notably the thermodynamic "wet get wetter" process of rainfall change (Held and Soden 2000, 2006; Allen et al. 2010; Christensen et al. 2013; Chou and Neelin 2004; Meehl et al. 2007; Chou et al. 2009; Seager et al. 2010). This operates at the largest scales (e.g., zonal means) and involves the increase in global specific humidity in a warmer atmosphere leading to an increase (decrease) in precipitation in the regions of mean moisture convergence (divergence). In the tropics this is likely to be offset by the weakening of the mean tropical overturning circulation associated with a reduction in convective mass flux in regions of present-day high ascent (Vecchi et al. 2006; Chadwick et al. 2013; Christensen et al. 2013; Ma and Xie 2013; DiNezio et al. 2013).

Chadwick et al. (2013, hereafter C13), however, proposed that the wet-get-wetter mechanism alone does not adequately explain the global pattern of multimodel mean (MMM) projected rainfall change. The spatial correlation of future precipitation change ΔP and mean precipitation P globally is low, such that at regional and seasonal scales in the tropics other processes dominate. These processes are substantially related to changes in the spatial location of moisture convergence and hence convection. These include dynamic effects of regional gradients in near-surface temperature change over oceans, that is, the "warmer get wetter" process (Xie et al. 2010), land–sea temperature contrasts (Dong et al. 2009; Byrne and O'Gorman 2013), land surface processes (Pitman 2003), aerosol direct, indirect, and semidirect effects (Huang et al. 2007; Lohmann and Feichter 2005; Ackerman et al. 2000; Hansen et al. 1997), and changes in circulation (Shepherd 2014). The thermodynamic balance of the "upped ante" (Neelin et al. 2003) mechanisms additionally contributes, leading to results such as the so-called modified warmer-get-wetter mechanism (Huang et al. 2013). The modified warmer-get-wetter mechanism is described as the combination of SST changes (the warmer-get-wetter effect) modified by background climatological moisture and SSTs due to the nonlinear relationship between tropical convection and SSTs.

Generally, the processes operating over the ocean are better understood than those over land but in all cases differing representation of these processes across models is likely to drive projection uncertainty. Most previous analyses have focused on the MMM projected change quantities; however, Rowell et al. (2015) highlighted the importance of understanding the mechanisms of change within individual models and concluded that further investigation should be aimed at developing expert judgment of process-based mechanisms and their reliability of projections (Rowell et al. 2015).

In this context, the aims of this paper are 1) to determine the mechanisms of projected regional precipitation changes by decomposition into thermodynamic and dynamic components; 2) to quantify the contribution to total ensemble projection uncertainty, as represented by

TABLE 1. CMIP5 model list of the 20 models used including modeling center, institute ID, and atmospheric resolution.

	Modeling center (or group)	Institute ID	Atmospheric resolution
BCC_CSM1.1(m)	Beijing Climate Center, China Meteorological Administration	BCC	2.8° × 2.8°
BNU-ESM	College of Global Change and Earth System Science, Beijing Normal University	GCESS	2.8° × 2.8°
CanESM2	Canadian Centre for Climate Modelling and Analysis	CCCma	2.8° × 2.8°
CCSM4	National Center for Atmospheric Research	NCAR	0.94° × 1.25°
CESM1(BGC) CESM1(CAM5)	Community Earth System Model contributors	NSF–DOE–NCAR	0.94° × 1.25°
CSIRO Mk3.6.0	Commonwealth Scientific and Industrial Research Organisation in collaboration with Queensland Climate Change Centre of Excellence	CSIRO–QCCCE	1.9° × 1.9°
FIO-ESM	First Institute of Oceanography, State Oceanic Administraion (SOA), China	FIO	2.8° × 2.8°
GFDL CM3 GFDL-ESM2G GFDL-ESM2M	NOAA/Geophysical Fluid Dynamics Laboratory	NOAA/GFDL	2.0° × 2.5°
GISS-E2-H	NASA Goddard Institute for Space Studies	NASA GISS	2.0° × 2.5°
HadGEM2-CC HadGEM2-ES	Met Office Hadley Centre (MOHC) [additional HadGEM2-ES realizations contributed by Instituto Nacional de Pesquisas Espaciais (INPE)]	MOHC (additional realizations by INPE)	1.25° × 1.9°
IPSL-CM5A-LR IPSL-CM5A-MR	L'Institut Pierre-Simon Laplace	IPSL	1.9° × 3.75° 1.25° × 2.5°
MIROC5	Atmosphere and Ocean Research Institute (The University of Tokyo), National Institute for Environmental Studies, and Japan Agency for Marine-Earth Science and Technology	MIROC	1.4° × 1.4°
MRI-CGCM3	Meteorological Research Institute	MRI	1.1° × 1.1°
NorESM1-M NorESM1-ME	Norwegian Climate Centre	NCC	1.9° × 2.5°

intermodel spread, associated with these mechanisms; and 3) to identify possible causes of uncertainty, and to draw inferences regarding the robustness and credibility of projected changes. The mechanism of change decomposition method of C13 is used to identify causes of precipitation change (aim 1) and associated uncertainty (aim 2) (reported in section 3a) and causes of uncertainty are inferred (aim 3) through analysis of the intermodel spread (reported in section 3b). This paper focuses on projected regional precipitation changes over southern Africa (SA) and the adjacent southwest Indian Ocean (SWIO) sector (0°–30°S, 10°E–80°E), where wet season rainfall is dominated by the SIOCZ (Cook 2000; Lazenby et al. 2016).

2. Data and methods

a. Data

We use output from simulations of the twentieth century and the twenty-first century [under the representative concentration pathway 8.5 (RCP8.5) emissions scenario] from 20 models [those used in Kent et al. (2015, Table 1 therein)] from the World Climate Research Programme (WCRP) CMIP5 multimodel dataset, which provide results for the most recent Fifth Assessment Report (AR5) of the Intergovernmental Panel on Climate Change (IPCC) (Meehl et al. 2007; Taylor et al. 2012) (see Table 1). We consider both the MMM of the 20 chosen CMIP5 models and the spread of model projections across the 20-model ensemble, to address aims 1 and 2 and aim 3, respectively. Lazenby et al. (2016) present the biases in the MMM of the larger full CMIP5 ensemble and we note that this is not significantly different from that of the MMM of the 20 CMIP5 models used here (see Figs. S1 and S2). Both MMMs represent well the dominant circulation features and the spatial structure of rainfall and its annual cycle. However, there is an overall positive precipitation bias compared to observations over the main climatological rainfall features over the Indian Ocean and central continent in austral summer, although not in the summer rainfall season over the Sahel zone (~15°N).

Monthly data were extracted for key diagnostic variables to understand potential physical processes linked to precipitation changes over the SA–SWIO sector. The period of analysis for projected climate changes is 2071–2100 (in the RCP8.5 experiment) minus the historical period 1971–2000. Only the first ensemble member was utilized in creating the MMM. All model data were interpolated to a common grid of 1.5° × 1.5° to ensure uniformity.

b. *The "mechanism of change" decomposition methodology*

To determine the main contributors to both the MMM precipitation change (see section 3a) and associated uncertainty (i.e., intermodel spread; section 3b) over the study domain, the C13 decomposition of change methodology was applied to data from each model for each calendar month. We then focus specifically on the early and main SA–SWIO wet seasons October–December (OND) and December–February (DJF), respectively.

Projected changes in precipitation can be decomposed into the dominant mechanisms of change, the thermodynamic and dynamic components. A number of methods have been proposed for the purpose (e.g., Seager et al. 2010; Emori and Brown 2005). We utilize the method of C13, which is based on the assumption that in convective climate regimes mean precipitation P is equivalent to the vertical mass flux from the boundary layer to the free troposphere M multiplied by specific humidity in the boundary layer q (Held and Soden 2006):

$$P = Mq. \tag{1}$$

As M (as defined here) is not directly available from most CMIP5 model outputs, in the decomposition a suitable surrogate M^* is derived directly from model mean P and q:under

$$M^* = \frac{P}{q}. \tag{2}$$

C13 demonstrated M^* to be a suitable replacement for actual column-integrated convective mass flux M_{int} at the gridpoint level in global climate models. Therefore, the projected precipitation change ΔP can be expressed as

$$\Delta P = \Delta(M^* q), \tag{3}$$

$$\Delta P = M^* \Delta q + q \Delta M^* + \Delta q \Delta M^*, \tag{4}$$

where M^* and q are the present day mean climatological values (1971–2000) of proxy mass flux and 2-m specific humidity respectively and ΔM^* and Δq are the projected changes in those quantities over the period 2071–2100 compared to 1971–2000.

In this formulation Δq and ΔM^* represent the thermodynamic and dynamic components of change, respectively. The C13 method has the advantage that the dynamical term ΔM^* can be further separated into $\Delta M^*_{\text{weak}}$and $\Delta M^*_{\text{shift}}$. The quantity ΔM^*_{weak} represents the tropics-wide weakening of the large-scale overturning circulation. It is derived from the climatological mean M^* ($\Delta M^*_{\text{weak}} = -\alpha M^*$), where α is a constant derived for each model, separately from the strong negative relationship observed between climatological M^* and ΔM^* across all grid cells in the tropics (assumed here to include all regions between 30°N and 30°S), that is, areas with higher M^* experience greater declines in ΔM^*, common to all models (see Figs. 3 and 6 from C13). The weakening in tropical circulation is due to the positive lapse-rate feedback response in which greater upper-level latent heating interacts with the mean circulation, leading to greater column warming in descent regions than ascent regions, thereby decelerating the tropical circulation (Ma et al. 2012). There is also a contribution to circulation weakening from the direct radiative effect of increased CO_2 concentrations (e.g., Bony et al. 2013).

Note that $\Delta M^*_{\text{shift}} = \Delta M^* - \Delta M^*_{\text{weak}}$; that is, the deviation in ΔM^* from that estimated directly from the regression of M^* and ΔM^* represents the effective "shift" at a given grid cell toward a greater or weaker convective mass flux.

The term Δq can also be further separated into two components:

1) Δq_{cc}, the Clausius–Clapeyron change in surface q for the change in mean 2-m temperature at each location (expected under fixed relative humidity), expressed as $\Delta q_{\text{cc}} = (\text{es}_2/\text{es}_1)q - q$, where es is the saturation vapor pressure and q is historical boundary layer specific humidity [the ratio expresses future (es_2) by historical (es_1) saturation vapor pressure], and
2) Δq_{rh}, the residual of $\Delta q - \Delta q_{\text{cc}}$, associated with changes in near-surface relative humidity.

On this basis ΔP for each model can be decomposed into its individual components as

$$\Delta P = M^* \Delta q_{\text{cc}} + M^* \Delta q_{\text{rh}} + q \Delta M^*_{\text{weak}} + q \Delta M^*_{\text{shift}} + \Delta q \Delta M^*, \tag{5}$$

which for convenience in terminology can then be expressed as

$$\Delta P = \Delta P_T + \Delta P_{\text{RH}} + \Delta P_{\text{Weak}} + \Delta P_{\text{Shift}} + \Delta P_{\text{Cross}}, \quad \text{where} \tag{6}$$

- ΔP is the change in precipitation expressed per degree global warming,
- $\Delta P_T - M^* \Delta q_{\text{cc}}$ is the thermodynamic change due to Clausius–Clapeyron-driven increases in specific humidity,
- $\Delta P_{\text{RH}} = M^* \Delta q_{\text{rh}}$ is the change due to near surface relative humidity changes,
- $\Delta P_{\text{Weak}} = q \Delta M^*_{\text{weak}}$ is the change due to the weakening tropical circulation,
- $\Delta P_{\text{Shift}} = q \Delta M^*_{\text{shift}}$ is the change due to spatial shifts in the pattern of convective mass flux, and

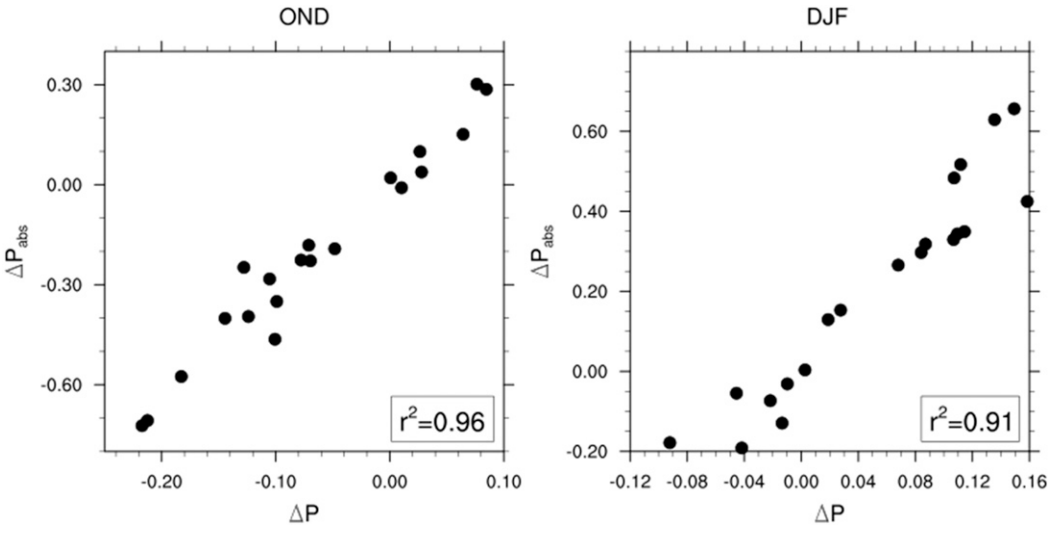

FIG. 1. Relation of absolute projected precipitation ΔP_{abs} change vs normalized precipitation change ΔP for the 20 CMIP5 models for the period 2071–2100 minus 1971–2000 under the RCP8.5 scenario for the seasons (left) OND and (right) DJF. Quantities are area averaged over the study domain (0°–30°S, 10°–80°E).

- $\Delta P_{\text{Cross}} = \Delta q \Delta M^*$ is the cross component of precipitation change, associated with interactions between the other components.

The total thermodynamic component consists of $\Delta P_T + \Delta P_{\text{RH}}$. For simplicity, we combine the total thermodynamic component ($\Delta P_T + \Delta P_{\text{RH}}$) with the dynamic component associated with the weakening of the tropical circulation (ΔP_{Weak}) to create a new component named ΔP_{twrh} [hereafter named the ''thermodynamic residual'' term, from Kent et al. (2015)]. We include ΔP_{Weak} with the thermodynamic terms due to the strong anticorrelation between these components. This analysis of the mechanisms of change as applied to the ensemble MMM is presented in section 3a.

c. *Analysis of uncertainty*

To quantify model uncertainty in projected change we assess the spread in the precipitation change components over the 20-model member ensemble (section 3b). The dominant spatial pattern of variation in ΔP_{Shift} between models is identified through EOF analysis, applied to the cross-model ΔP_{Shift} fields (standardized) for two separate domains within our study region: the southern African continental land region (10°–30°S, 10°–40°E) and the Indian Ocean (0°–30°S, 40°–80°E) region, (see section 3c). Potential drivers of this uncertainty are then assessed through correlations of the ΔP_{Shift} EOF component scores with diagnostic fields (SST and circulation indices) across the model ensemble and through composite analysis of diagnostic fields from models, sampling the upper and lower 25% of models from the EOF scores (see section 3c).

Note that all components of projected change in this analysis are normalized by the mean global surface temperature change ΔT_{global} of each individual model, and therefore all quantities are expressed as per degree of global warming. This removes the uncertainty due to intermodel spread in climate sensitivity and makes results scalable to the magnitude of warming (assuming quasi-linearity of regional precipitation change with warming) and therefore tractable when applied to predefined warming levels for policymakers. Removing the effect on ΔP of uncertainty in model ΔT_{global} related to model climate sensitivity (i.e., the high correlation between normalized and absolute precipitation changes; see Fig. 1) indicates a minor influence on our results.

3. Results and discussion

a. *Changes in multimodel mean precipitation over southern Africa and the adjacent Indian Ocean*

First, we consider the annual cycle of zonally averaged MMM precipitation changes over our study domain for land and ocean regions (Figs. 2a and 2b, respectively). The most pronounced feature of projected changes in rainfall over both land and ocean is an opposing dipole of future wetter and drier conditions, oriented to the north and south, respectively, of the climatological axis of maximum rainfall. However, the drying–wetting dipole is not obvious in January–February (Fig. 2a), particularly over land. This ΔP wetter–drier dipole structure effectively straddles the ITCZ with wetting (feature A in Figs. 2a,b) and drying (feature B in Figs. 2a,b) located to the north and south, respectively,

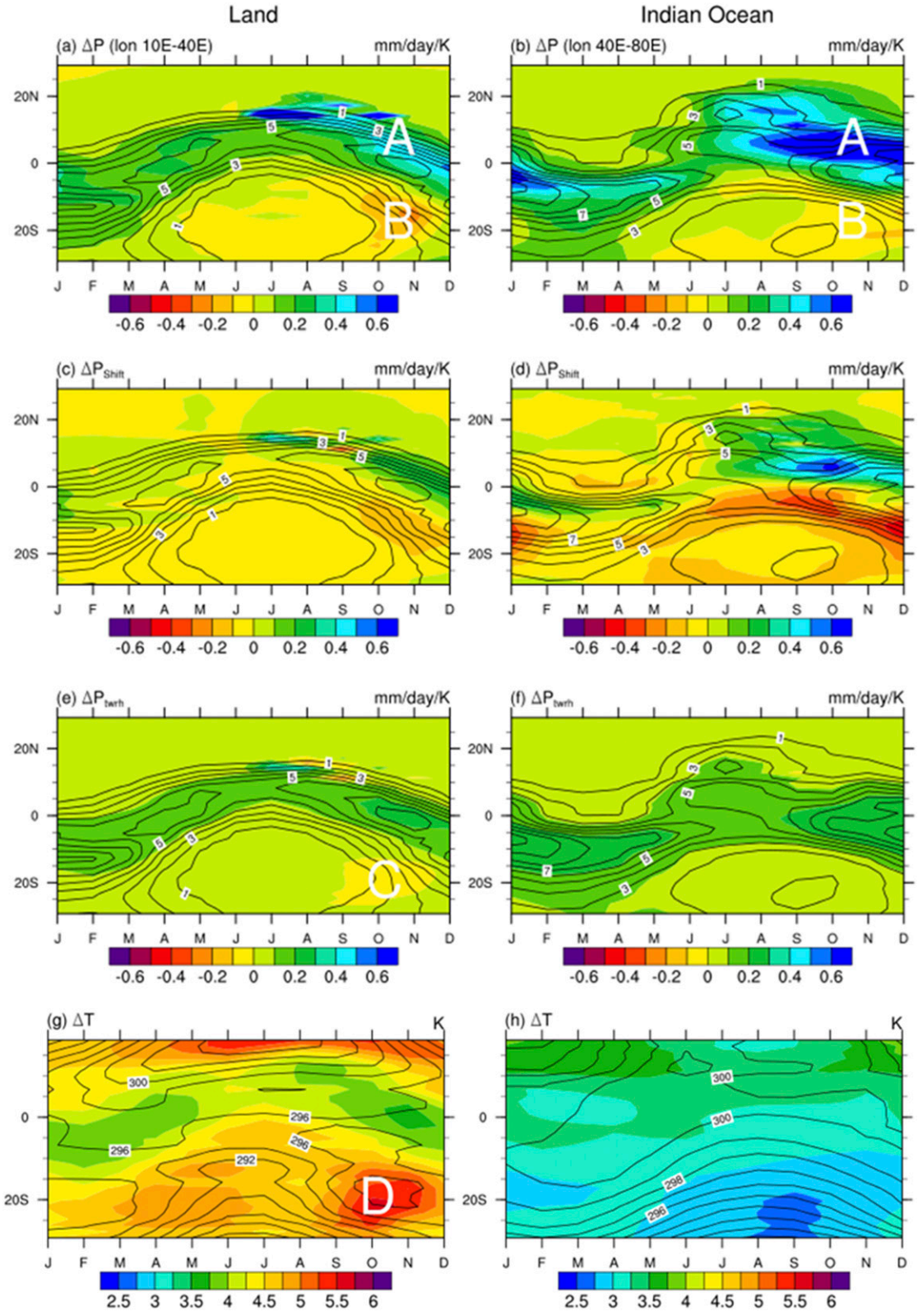

FIG. 2. Time–latitude plots of projected MMM changes in precipitation, and related mechanisms of change components, derived from the 20 CMIP5 models for the future period 2071–2100 minus 1971–2000 under the RCP8.5 scenario. Values

of the ITCZ axis. This indicates an effective northward shift in the ITCZ. This dipole pattern, however, has a strong seasonal cycle peaking in austral spring (September–December) over both land and ocean. The OND season is often overlooked in studies of SA–SWIO climate in favor of the main rainy season, DJF, but here we note a remarkably strong rainfall change signal in OND.

The spatial patterns of MMM precipitation change over our study region for the key seasons OND and DJF (Figs. 3 and 4) clearly illustrate this dominant zonally oriented pattern of wetter (drier) conditions located to the north (south) of the mean ITCZ at ~10°S, apparently connecting precipitation changes over the southern African continent with those in the equatorial and southwest Indian Ocean. The continental drying is most pronounced in OND (Fig. 2a, feature B) centered at ~15°S over the southern African continent. This may indicate a later start and reduced length of the growing season rainfall with serious implications on the agricultural sector. In addition to the wetting–drying dipole there is evidence of additional wetting over 25°–30°S over eastern South Africa and across into the southwest Indian Ocean, especially in DJF.

The decomposition can aid in understanding the processes driving these changes. The thermodynamic component ΔP_T (Figs. 3d and 4d) results in a wetting signal everywhere but whose magnitude is proportional to a rise in temperature through the Clausius–Clapeyron relation (i.e., it represents the wet-get-wetter process and maps substantially onto mean rainfall). It is substantially offset by an equivalent pattern of drying from the weakening of the tropical overturning circulation ΔP_{Weak} (Figs. 3e and 4e), which is inversely proportional to M^* and as such maps onto mean P. In addition, over land wetting from ΔP_T is offset by drying from ΔP_{RH} (Figs. 3f and 4f), due to reduced relative humidity, presumably resulting from moisture supply not keeping pace with increasing temperature. Together, these terms constitute the thermodynamic residual term ΔP_{twrh} (Figs. 2e, 2f, 3g, and 4g), which drives a net wetting signal, peaking over the oceanic climatological ITCZ and humid land regions. Therefore, ΔP is partly composed of a thermodynamic wet-get-wetter process magnifying the mean ITCZ rainband. However, the thermodynamic ΔP_{RH} response also drives up to ~50% of the drying over subtropical land regions during OND (feature C in Fig. 2e) centered on ~20°S. This is broadly coincident with the maxima in ΔT (Fig. 2g, feature D), suggestive of a land–atmosphere positive feedback response in early wet season, which is overcome during the peak DJF wet season. As such over land in OND ΔP_{twrh} is an important driver of the spatial pattern of ΔP ($r = 0.70$, where r is the spatial correlation), substantially associated with ΔP_{RH}.

However, over the study region as a whole, it is clear from Figs. 2–4 and Table 2 that the spatial pattern of ΔP in OND or DJF is not closely related to that of mean precipitation (P) (spatial correlations are not significant at the 95% confidence interval) or to the thermodynamic residual term ΔP_{twrh} ($r = 0.46$ and 0.30 for OND and DJF, respectively), such that the notable dipole features of ΔP are not driven by the wet-get-wetter process. Rather, ΔP most closely matches the dynamical component ΔP_{Shift} ($r = 0.94$ for OND and 0.96 for DJF) such that it is changes in the location of convection that explain the dipole. Note that ΔP_{Shift} contributes most of the wetting–drying dipole over land and almost all of it over ocean, especially the drying signal south of the ITCZ. We postulate here that this projected northward shift of the ITCZ over the Indian Ocean may be related to projected changes in the SST structure through a "warmest get wetter" mechanism. The north–south gradient in SST over the Indian Ocean, which is broadly representative of the ΔP dipole [~(5°N–20°S)] in the present day of ~(2–4) K over the austral summer–winter seasons (Fig. 2h), is enhanced in the MMM projections by ~0.5 K (Figs. 2h, 3h, and 4h). This may lead to a northward displacement of convection toward the warmest oceanic waters, similar to that noted for the tropical Pacific (Widlansky et al. 2013).

b. *Quantifying uncertainty in projected change in precipitation: Ensemble spread*

Uncertainty across the multimodel ensemble remains a feature in projections of future precipitation across the tropics and is a major barrier to effective use of climate information in adaptation activities, notwithstanding approaches to "decision making under climate uncertainty" (e.g., Lempert and Collins 2007). Here, we

←

are averaged over longitude bands indicative of (left) the SA continent (10°–40°E; land only) and (right) the Indian Ocean (40°–80°E; ocean only). (a),(b) ΔP (shaded) overlaid with historical climatological P (1971–2000). (c),(d) As in (a),(b), but for ΔP_{Shift} (shaded). (e),(f) As in (a),(b), but for ΔP_{twrh} (shaded). (g),(h) ΔT overlaid with historical climatological T. (Units of ΔP and associated components are in mm day^{-1} K^{-1} global warming and P in mm day^{-1}. Units of ΔT and T are in kelvin. See text for explanation of features marked with A–D.)

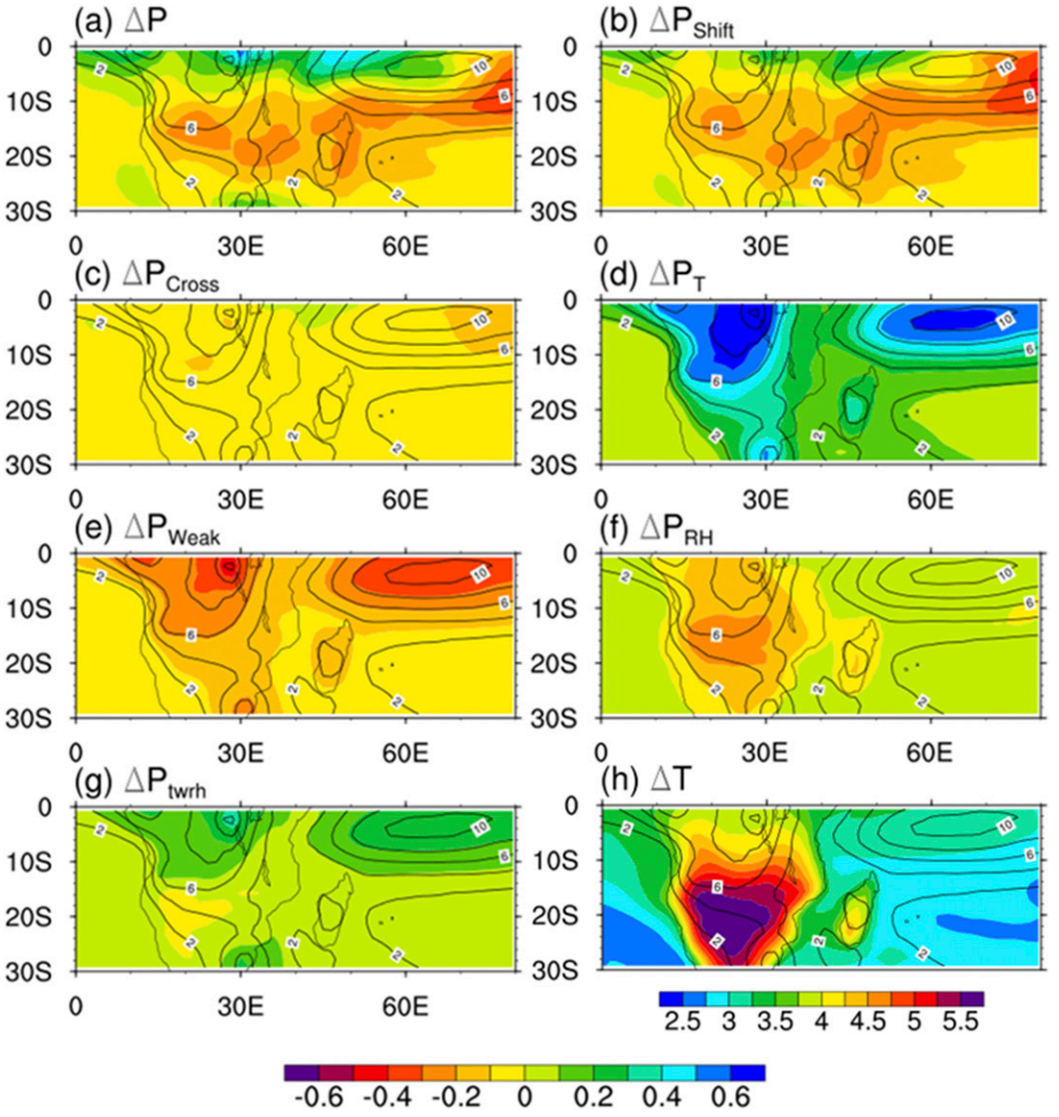

FIG. 3. (a) Projected MMM changes in precipitation, and (b)–(g) related mechanisms of change components, derived from the 20 CMIP5 models for the future period 2071–2100 minus 1971–2000 under the RCP8.5 scenario, for the OND season over SA and the SWIO region. The ΔP_{twrh} is the sum of $\Delta P_T + \Delta P_{\text{Weak}} + \Delta P_{\text{RH}}$. Black contours overlaid represent climatological precipitation for the specific season contoured from 0 to 10 mm day^{-1} in intervals of 2 mm day^{-1}. Units are in absolute change per kelvin global warming. (h) Projected 20 CMIP5 MMM temperature changes for the same time period and region (K).

assess the contributions to total ensemble uncertainty from the various mechanisms of change in our decomposition. We assess the robustness of projected changes from the magnitude of intermodel spread for each component as represented in two forms: first as maps of the standard deviation of the ensemble at each grid cell (Figs. 5 and 6) and second as box-and-whisker plots of intermodel spread for each component averaged over specific regions of interest (Fig. 7). We average over areas where the MMM change signal shows mean future wetting or drying to help inform interpretation of the robustness of key signals emerging from MMM commonly used (e.g., Flato et al. 2013; IPCC 2013). Further, we consider land and ocean separately given the differing level of importance for adaptation actions and differing mechanisms driving changes. A number of broad signals emerge.

(i) Changes in precipitation averaged over the regions of wetting–drying from the MMM are more robust over land than ocean for both the future wetting and drying signals (i.e., total uncertainty in ΔP is

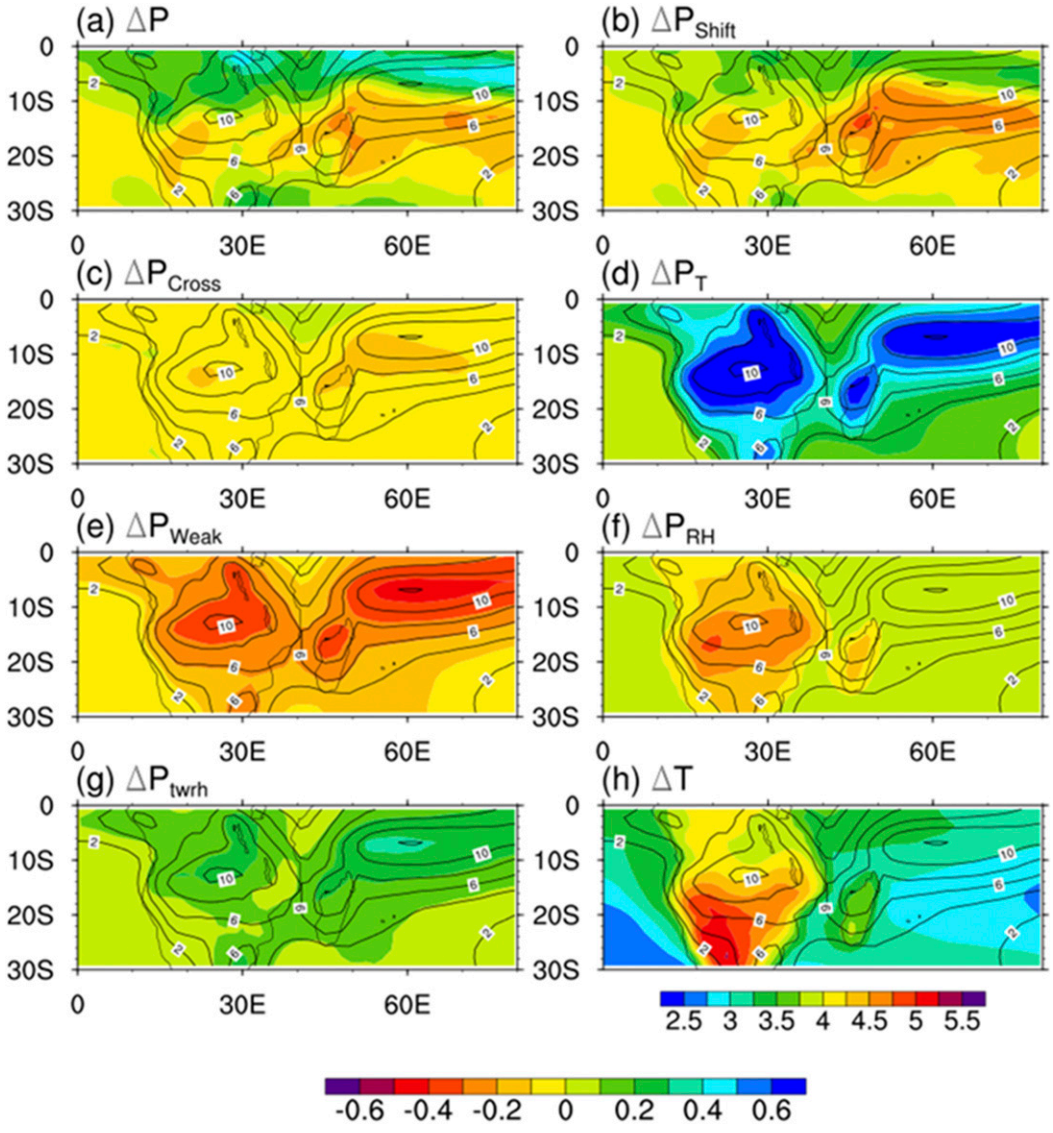

FIG. 4. As in Fig. 3, but for the DJF season.

lower for land compared to ocean; Fig. 7). This difference in the spread of ΔP is largely related to that in ΔP_{Shift} ($r = 0.95$ for OND and 0.97 for DJF for land regions), such that uncertainty in the dynamical drivers of projected change is dominant. We consider the contribution of intermodel differences in SST structures to uncertainty in ΔP_{Shift} in section 3c.

(ii) The MMM projected drying is more robust than wetting over both land and ocean and in OND, but differences are small in DJF. The future signal with the greatest robustness is the continental drying over (especially western) SA during the OND season (Figs. 5 and 7), reinforcing the importance of this early wet season component of the larger-scale rainfall change dipole. During DJF (Figs. 6 and 7) the MMM drying signal is less robust, and there are "hotspots" of nonrobust change, which include parts of Malawi, Tanzania, Madagascar, and northern Mozambique, with potentially important implications for approaches to climate change adaptation. Areas of robust wetting include East Africa and the western Indian Ocean at the equator.

(iii) The local hotspots in intermodel ΔP standard deviation show that uncertainty in ΔP does not simply scale with the absolute magnitude of ΔP. These are located, for example, proximate to the African great lakes, regions of complex topography (e.g., Madagascar), and at the transition boundaries of wetting and drying over the Indian Ocean (Figs. 5a

TABLE 2. Spatial correlations of MMM ΔP vs the different mechanisms of change components for both DJF and OND for the SA–SWIO region (0°–30°S, 10°–80°E). (Using the Student's t test correlation values above 0.44 are deemed significant at the 95% confidence interval, shown in boldface.)

DJF	ΔP (0°–30°S, 10°–80°E)	ΔP Land (0–30°S, 10°–40°E)	ΔP Ocean (0°–30°S, 40°–80°E)	OND	ΔP (0°–30°S, 10°–80°E)	ΔP Land (0°–30°S, 10°–40°E)	ΔP Ocean (0°–30°S, 40°–80°E)
ΔP_{Shift}	**0.96**	**0.97**	**0.97**	ΔP_{Shift}	**0.94**	**0.95**	**0.95**
ΔP_T	0.18	0.04	0.24	ΔP_T	0.29	0.26	0.29
ΔP_{Weak}	−0.23	−0.16	−0.29	ΔP_{Weak}	−0.35	−0.39	−0.33
ΔP_{RH}	0.12	0.40	0.30	ΔP_{RH}	0.21	**0.46**	**0.54**
ΔP_{twrh}	0.30	**0.53**	0.27	ΔP_{twrh}	**0.46**	**0.70**	0.33
ΔP_{Cross}	**0.57**	**0.51**	**0.58**	ΔP_{Cross}	0.35	0.19	0.43
P	0.18	0.12	0.22	P	0.30	0.34	0.27

and 6a), which raises the possibility that intermodel differences in background climatology may project onto the uncertainty in ΔP. However, only some of these hotspots of uncertainty correspond to locations of high intermodel spread in mean P (Figs. 5h and 6h), such that most of the spatial pattern in uncertainty in ΔP is unrelated to background climatology. The high uncertainty in ΔP often apparent in wetting–drying transition zones suggest that caution needs to be attached to interpretation of near-zero MMM ΔP change.

(iv) Most of the total uncertainty in ΔP is contained in the ΔP_{Shift} component, whose uncertainty is typically greater by a factor of 2–4 than that of the thermodynamic residual. Intermodel standard deviation within the ΔP_{Shift} term is markedly higher over ocean than land, notably over the ΔP dipole region. While the MMM wetting–drying dipole over the Indian Ocean may result from a warmest-get-wetter response to changes in the SST structure (Figs. 5h and 6h), high uncertainty in ΔP_{Shift} suggests strong intermodel divergence in the form of the ΔSST patterns responsible (Chadwick 2016), which we explore in section 3c. Indeed, in many regions, notably the region of projected drying over the Indian Ocean at 10°–15°S, the model uncertainty in ΔP_{Shift} is higher than that in ΔP. Note that ΔP_{twrh} is especially robust over the ocean ITCZ where the thermodynamic response is closest to that of ΔP_T.

(v) Since the total uncertainty can be less than the sum of the individual components (e.g., Fig. 7) we can infer that the intermodel components are anticorrelated across models and offset each other, which acts to constrain total uncertainty in ΔP. For the drying over continental SA (during OND) and to a lesser extent over the Indian Ocean, uncertainty in the dynamical ΔP_{Shift} and thermodynamic residual term ΔP_{twrh} terms appear to offset each other, resulting in a total intermodel standard deviation of ΔP, which is much less than the sum of the component terms.

(vi) The thermodynamic change due to Clausius–Clapeyron-driven increases in specific humidity (ΔP_T) exhibits the largest magnitude of all the decomposed components (Fig. 7); however, this is largely offset by the weakening of the tropical circulation component (ΔP_{Weak}) and relative humidity component (ΔP_{RH}) over land regions.

c. *Understanding potential causes of uncertainty in the dynamic component of projected change*

The dynamical ΔP_{Shift} term provides the primary contribution to intermodel uncertainty in future projections of precipitation. Among the potential causes of this uncertainty in the location of tropical convection, a primary candidate is the varying patterns of model projected SST changes. We explore this using EOF analysis of the intermodel ΔP_{Shift} patterns. Over the Indian Ocean domain during both OND and DJF the leading mode of intermodel ΔP_{Shift} variability shows a loading pattern (Figs. 8a,b) that projects strongly onto the pattern of the future wetting–drying dipole in ΔP_{Shift} (Figs. 3b and 4b), and indeed in ΔP explaining 37% and 31.5% of variability, respectively. These EOFs therefore represent well the strength of the MMM ΔP wetting–drying dipole, oriented broadly north–south, in individual models.

The component scores of this leading EOF correlate moderately with intermodel ΔSST over the Indian Ocean in both OND and DJF (Figs. 8c,d). In both cases the correlation is such that a stronger north–south wetting–drying dipole in individual models is associated with lower rates of SST warming in the Indian Ocean south of the equator, and hence an increased north–south SST gradient across the Indian Ocean. This response across models is consistent with the warmest-get-wetter mechanism inferred from the MMM changes in precipitation and SST (section 3a).

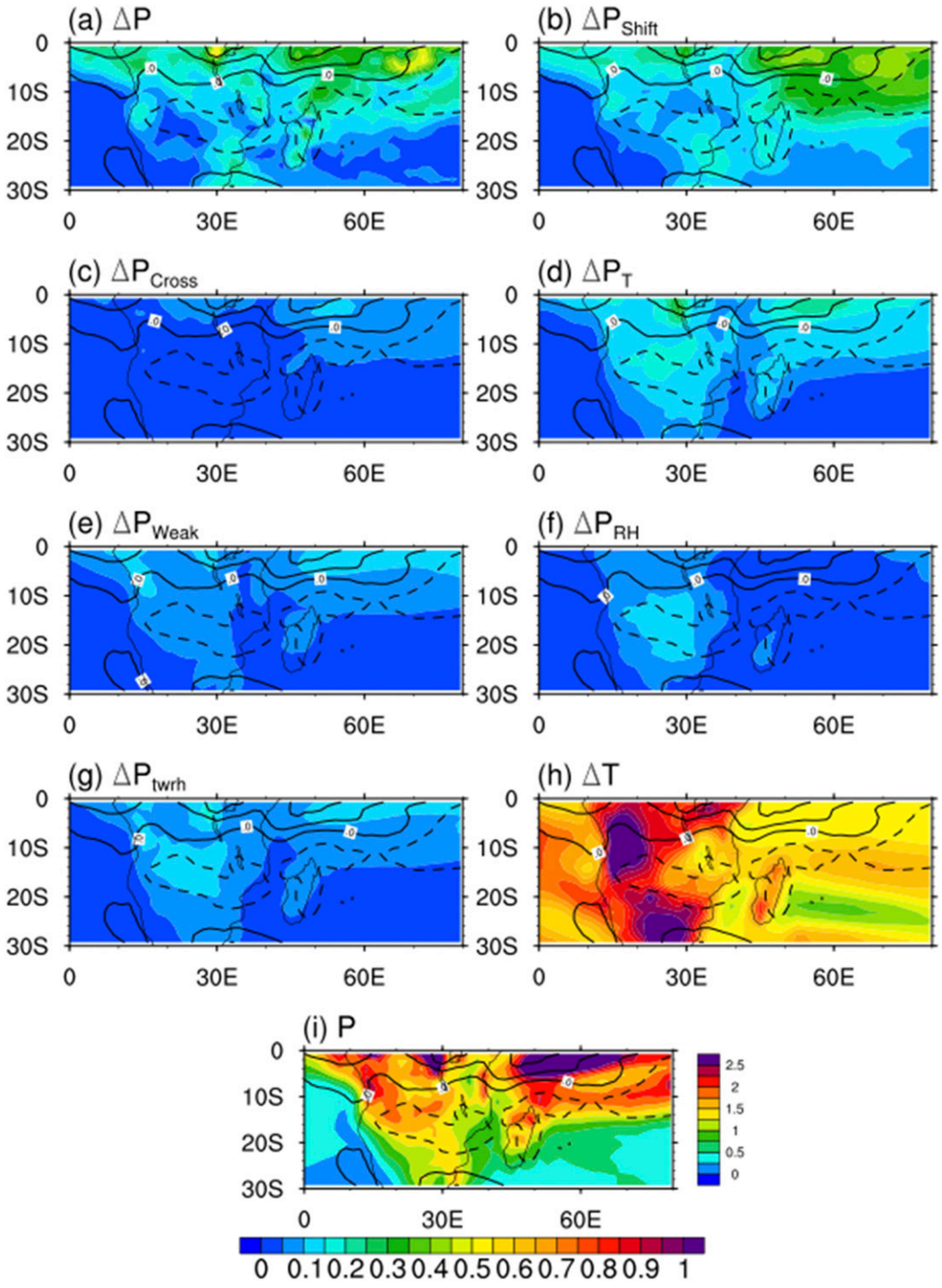

FIG. 5. Intermodel standard deviation (shaded) in (a) ΔP (mm day^{-1} K^{-1}) and (b)–(g) mechanism of change components therein (mm day^{-1} K^{-1}), (h) ΔT (K), and (i) P (mm day^{-1}), for the OND season. Contours show MMM ΔP (values from −0.6 to 0.6 mm day^{-1} K^{-1} in intervals of 0.2, where dashed contours show negative values). Change quantities are for the period 2071–2100 minus 1971–2000 under the RCP8.5 scenario.

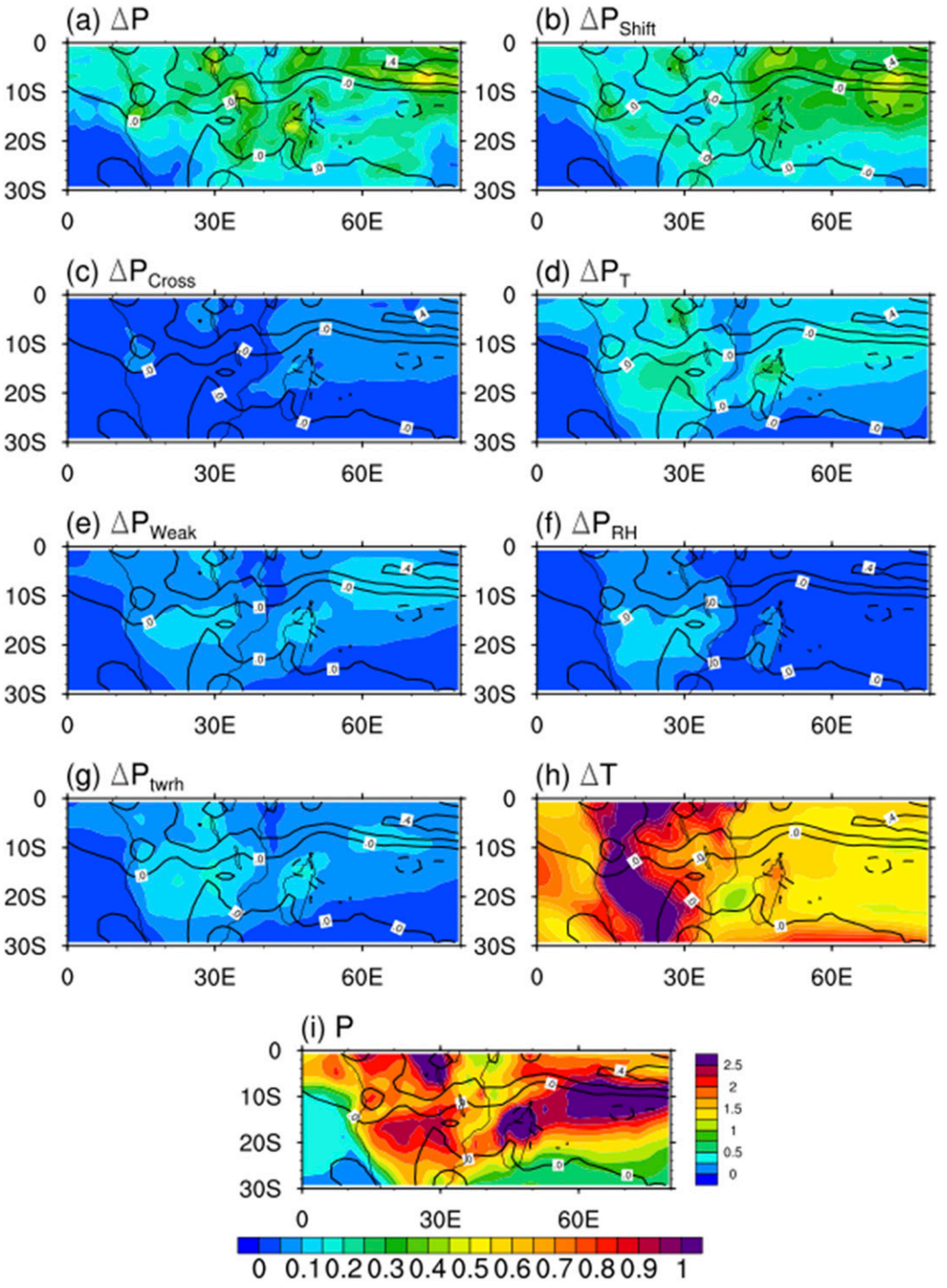

FIG. 6. As in Fig. 5, but for DJF.

Moderate correlations also exist with ΔSST in the tropical Pacific broadly around the Niño-3.4 region. During OND there is an additional indication that the ΔP_{Shift} EOF dipole is related to changes in the mean east–west SST gradient reminiscent of the Indian Ocean dipole (IOD) mode of interannual variability active in this season (Saji et al. 1999). Previous analysis has related changes in long-term mean precipitation to a shift toward a preference for the positive mode of the IOD in some coupled models (Shongwe et al. 2011),

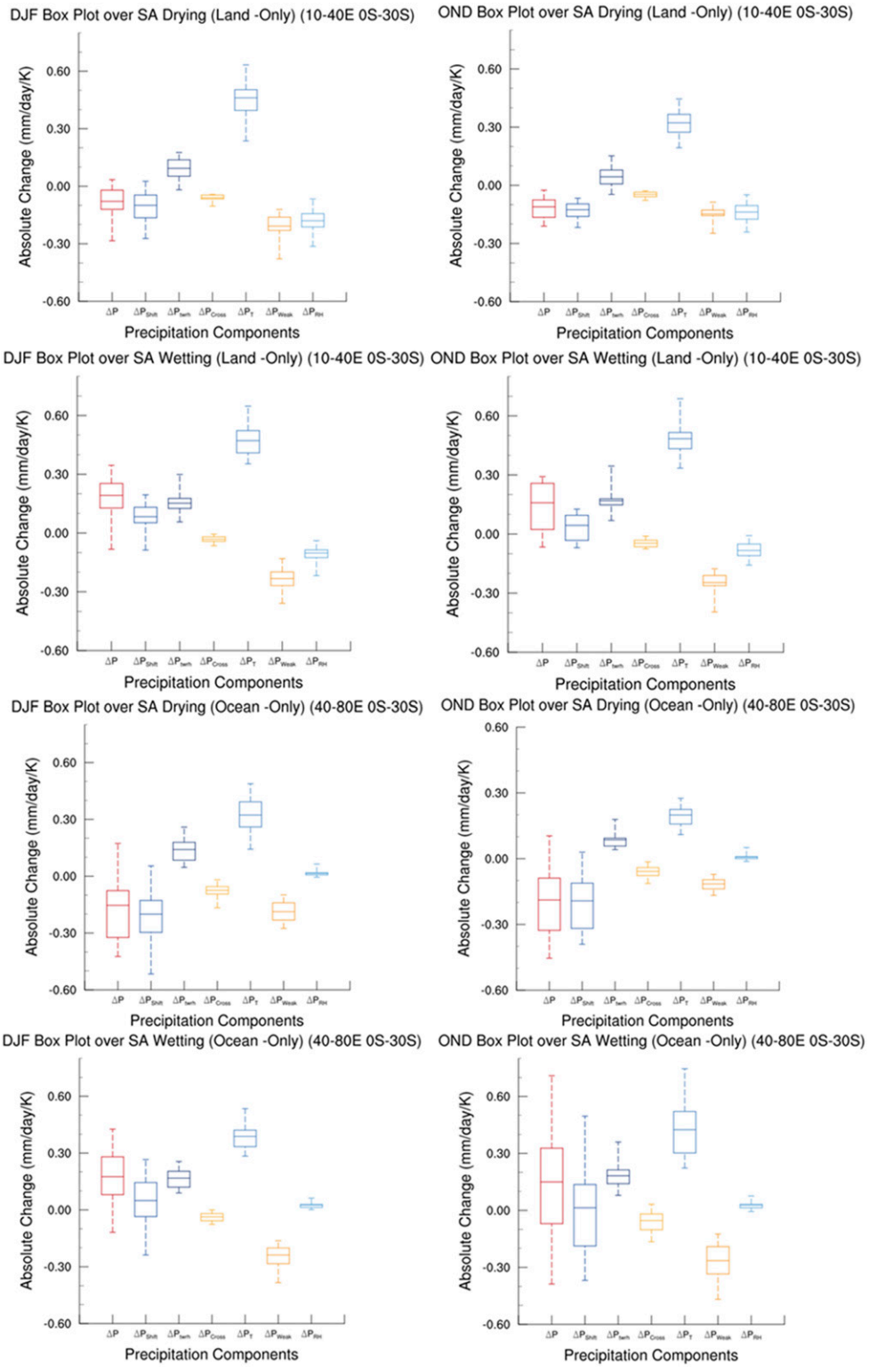

FIG. 7. Box-and-whisker plots of the future change in ΔP and various components therein from the 20 CMIP5 models, for the period 2071–2100 minus 1971–2000 for RCP8.5 of CMIP5 models for (top)–(bottom) drying and wetting (land only) and drying and wetting (ocean only) for (left) DJF and (right) OND. (Units are in mm day^{-1} K^{-1} global warming.)

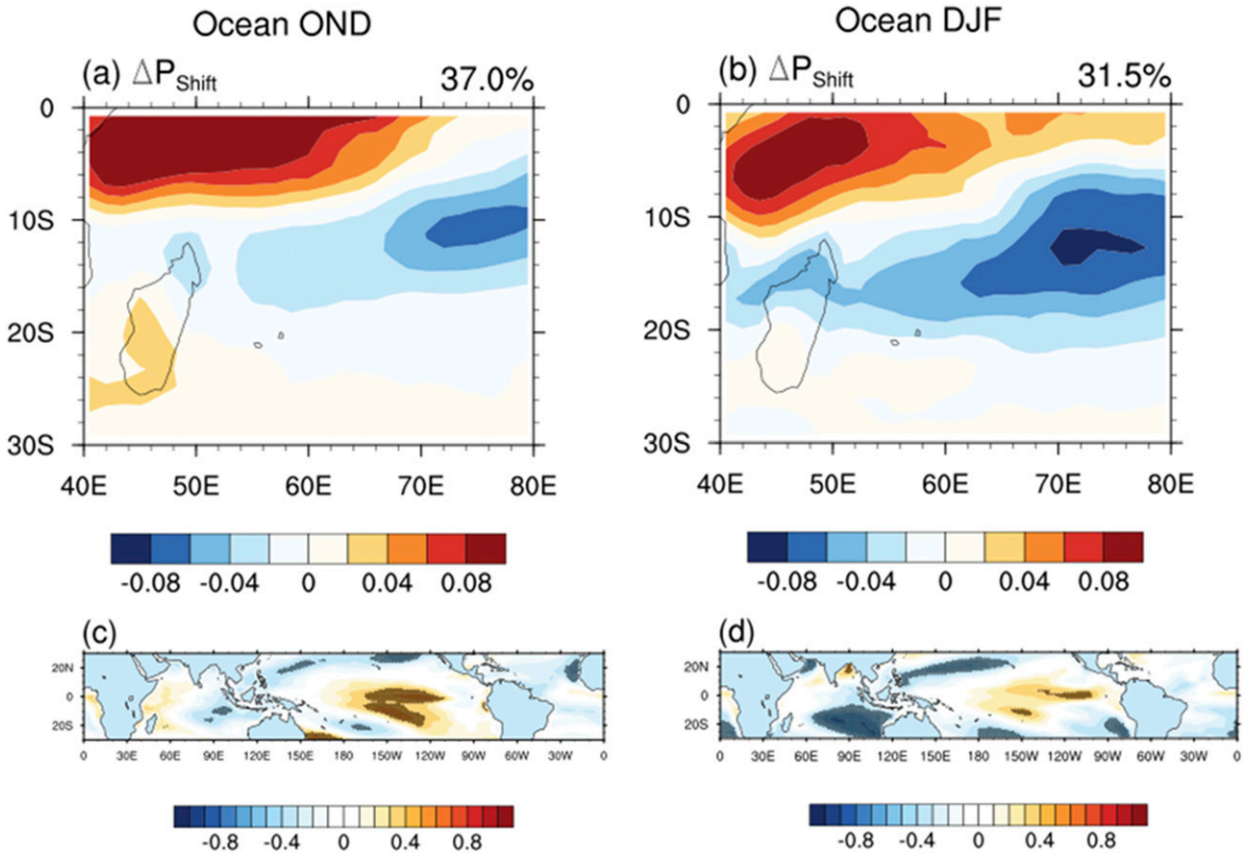

FIG. 8. (a),(b) Leading EOF loading patterns of intermodel ΔP_{Shift} for 20 CMIP5 models over the Indian Ocean domain for OND and DJF, respectively; and (c),(d) the respective correlation coefficients of the EOF component scores vs intermodel ΔSST. Significant correlations at the 90% percentile are stippled.

which remains consistent with the warmest-get-wetter mechanism.

Over the domain centered on the SA landmass the intermodel ΔP_{Shift} EOF analysis for both the OND and DJF seasons reveals a dominant EOF loading pattern oriented diagonally northwest–southeast across SA toward the southwest Indian Ocean (Figs. 9a,b). The peak loadings lie to the southwest of the position of the mean SIOCZ feature such that the EOF represents the magnitude of the MMM drying signal to the south of the mean rainfall maximum. The MMM projected pattern of ΔP_{Shift} change across the region is more zonally oriented than the EOF SIOCZ-like orientation (Figs. 3b and 4b; see section 3a) such that the MMM change clearly masks considerable spread within the ensemble.

The EOF pattern of intermodel ΔP_{Shift} appears associated with intermodel variability in SST, land heating and circulation and resulting moisture fluxes based on both correlations (Figs. 9c,d) and composites of diagnostic fields based on samples of the upper and lower 25% of models from the EOF component scores (Fig. 10). The EOF is rather weakly correlated to the intermodel structures of projected changes to SST across the southern Indian Ocean with an east–west dipole structure of correlation with the EOF component scores along ~(20°–25)°S (Figs. 9c,d) and corroborated in the composites (Fig. 10). For both the OND and DJF EOF, stronger future drying over SA in models is associated with weaker future warming in the Mozambique Channel–southwest Indian Ocean and stronger warming in the eastern subtropical Indian Ocean, as well as the eastern South Atlantic.

While the spatial patterns are similar, the correlations of EOF and SST are notably stronger in DJF than OND (Figs. 8c,d and 9c,d). The implication is that SSTs are most significant in austral summer than the transition season over the southern African region, particularly over the South Atlantic Ocean and central Indian Ocean. OND rainfall does not exhibit sufficient evidence of a significant link with changing SST gradients. Reason et al. (2006) state that the onset of the wet season over southern Africa appears to be associated with anomalous ridging of the South Atlantic high pressure, which requires further investigation and may shed more light on this research.

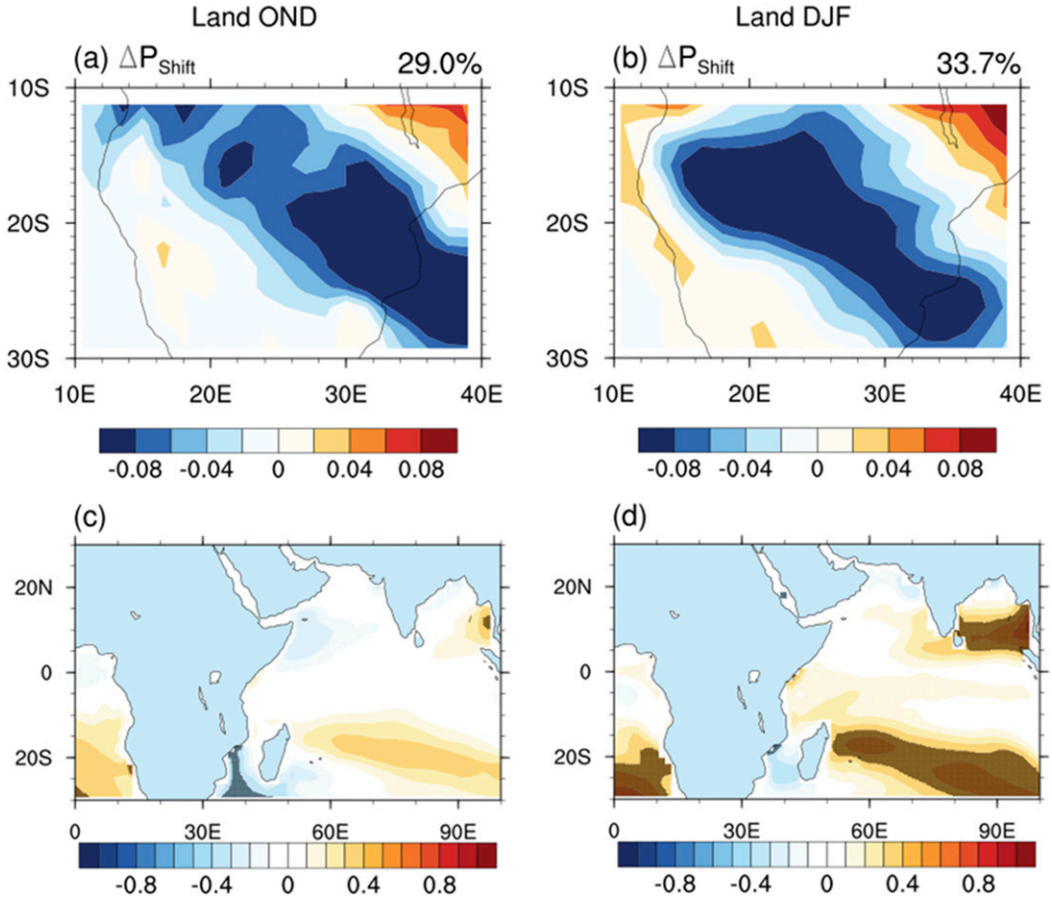

FIG. 9. As in Fig. 8, but for the southern Africa land domain whereby ΔSST correlations are restricted only to the SWIO domain.

Circulation features associated with the intermodel spread are identified by compositing projected changes in diagnostic fields in the top and bottom 25% of models from the EOF coefficients (Fig. 10). We find that in both seasons more intense versus weaker drying over SA in models is associated with cyclonic low-level circulation over the southwest Indian Ocean (Fig. 10) around a relatively weaker subtropical high, resulting in weaker Indian Ocean easterlies, and therefore an effective northeastward shift in the axis of the SIOCZ (Lazenby et al. 2016). In DJF (Fig. 10b) intense drying is also favored in models in which strong land heating occurs at ~20°S. This may be a result of reduced soil moisture but the heating drives an apparent intensification of the continental low-pressure center (the "Angolan low" feature) and cyclonic low-level circulation. While this might be expected to favor rainfall over the continent, the composite of the drier models (not shown) indicates a marked anomalous southward shift of the low with implications for moisture transport. There is some indication of an intensified South Atlantic anticyclonic circulation in the models with more intense drying whose link with the SST changes requires further investigation.

These structures of intermodel differences in ΔSST, land temperature, and low-level circulation that may drive the leading pattern of intermodel spread in ΔP_{Shift} over SA have some resonances with modes and structures of interannual variability in the region. Notable among these are the following. (i) The first is the regional response to ENSO characterized by the displacement in the SIOCZ associated with cyclonic low-level anomalies over the southwest Indian Ocean during El Niño events (Cook 2001), similar to that in Fig. 10. However, it is cautionary to note that the physical mechanisms and influence of local Indian Ocean SST (e.g., Goddard and Graham 1999) versus remote Pacific SSTs (e.g., Cook 2001; Ratnam et al. 2014) in driving this in the observed climate remain to be fully resolved. (ii) The second feature is the south Indian Ocean dipole (SIOD) mode of east–west SST gradient in the subtropical Indian Ocean (Behera and Yamagata 2001). In

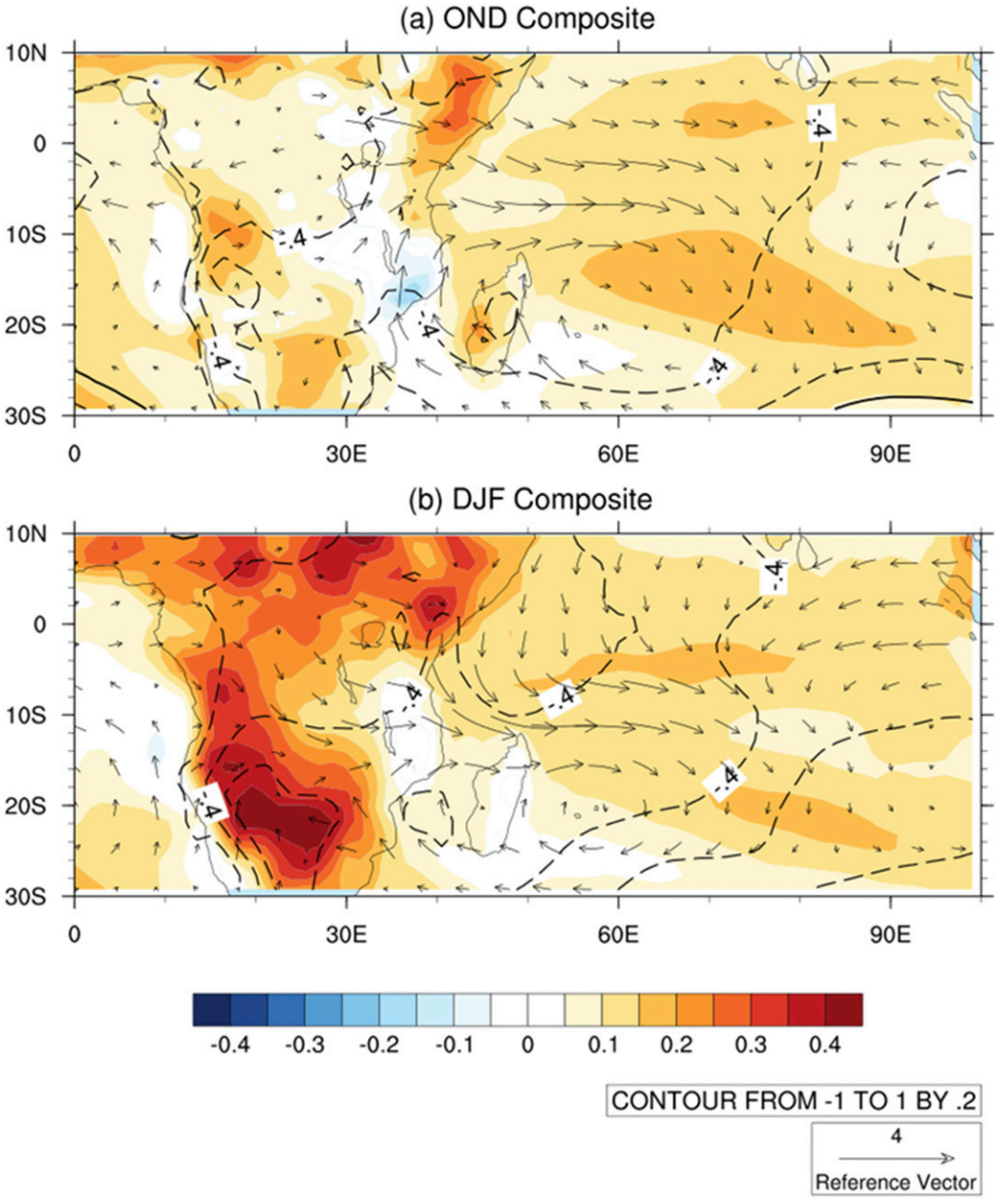

FIG. 10. Composite mean fields of diagnostic variables based on samples of the uppermost 25% minus the lowermost 25% of models selected from the component scores of the leading EOF of the intermodel ΔP_{Shift} (Figs. 9a,b) for (a) OND and (b) DJF. Fields shown are changes in surface temperature (K; shaded), surface pressure (hPa; contours, interval 0.2), and 850-hPa OND winds (m s^{-1}; vectors).

this case, although the form of the association of ΔP_{Shift} over SA and ΔSST matches that of interannual variability in SA rainfall and the phase of the SIOD (Reason 2001), the circulation responses diverge (Fig. 10). (iii) Finally, there is the intensity of the Angolan low and associated circulation changes, known to be an important control on present day precipitation in observations (e.g., Manhique et al. 2011) and in models (Munday and Washington 2017). During wet (dry) years the strength of the Angola low tends to be stronger (weaker) with enhanced (suppressed) circulation bringing in moisture from the Atlantic and the Indian Ocean (Cook et al. 2004; Munday and Washington 2017). Differential rates of future warming over land versus ocean may be expected to intensify and displace the Angolan low and we see evidence of differential response across models

strongly related to intermodel uncertainty in the structure of future dynamical precipitation responses.

Of course, we would not expect the dynamical processes of intermodel spread in projected rainfall change to be consistent with all aspects of current interannual variability, given (i) the complex suite of interannual modes affecting the SA region and (ii) the highly variable and mixed ability of coupled models to represent the mean state and variability, both through local processes (Lazenby et al. 2016) and remote teleconnections (e.g., Rowell 2013). Nevertheless the link between processes of climate variability and projected change has proved to be a fruitful focus in recent years in explaining why models make the future changes they do, providing some basis for assessing potential credibility of projected change.

4. Summary and conclusions

Human influence is expected to drive considerable changes to the hydrological cycle, of particular concern in regions such as southern Africa that are currently vulnerable to climate. There is a need to quantify and understand the projections of future precipitation change and associated uncertainty to inform the possible use of climate information in adaptation planning (Hackenbruch et al. 2017). Our analysis of end-of-twenty-first-century projections from a sample of 20 models from the CMIP ensemble reveals a dominant dipole pattern of precipitation change over SA and the SWIO with a wetting (drying) response to the north (south) of the ITCZ, with therefore an effective northward shift in the ITCZ. Pronounced drying is exhibited over land in OND, implying a delay in the onset of the wet season, an important and relatively robust signal.

A decomposition framework is applied to separate the mechanisms of change in both the MMM and in individual models to shed light on the relative importance of the multiple, coincident, and often competing mechanisms that may drive future precipitation changes in a warmer world. We show that the dynamical component ΔP_{Shift} representing spatial shifts in convection explains most of the dipole structure of ΔP, as evidenced by high spatial correlations no less than 0.94 over the study domain. The thermodynamic component of increased moisture is offset by the weakening of the tropical circulation leading to a relatively weak wet-get-wetter contribution. Considering the robustness of projected change, represented by the intermodel dispersal in response, we find that ΔP_{Shift} holds the most uncertainty, whereas the thermodynamic component is typically more robust. Drying is more robust than wetting over the continent, notably in the early summer OND season.

For both the OND and DJF seasons MMM future precipitation projections show, at the broadest scale, a wetting–drying dipole across the continent and Indian Ocean. Over land the magnitude, extent, and robustness of drying is greater during in OND than DJF, with implication of a later onset in the wet season over southern Africa. Greater uncertainty during DJF is apparently associated with a stronger role of intermodel differences in the structure SST changes in the adjacent oceans.

Over the Indian Ocean sector, we relate the dominant dynamically driven ΔP_{Shift} component to changes in SST structures. The wetting–drying dipole is associated with patterns of SST change, both in the MMM and across the model ensemble, that is consistent with a warmest-get-wetter mechanism driving the northward shift in the location of convection and convergence. Much of the model uncertainty is therefore associated with intermodel differences in future SST patterns in the tropical Indian and Pacific Ocean and the atmospheric teleconnection response, such that better understanding of these projected changes and in the teleconnections linking these to rainfall may provide some basis for constraining uncertainty in projections. This inference, however, is particularly applicable to DJF as OND does not exhibit the same magnitude of significance over the region.

Changes in rainfall over land are likely more complex, first because over the continental interior of SA the contribution to mean drying of the thermodynamic reduction in relative humidity is roughly equal to that of the dynamical component. Reduced relatively humidity is likely itself to be related to the effects of enhanced land–sea temperature contrasts and physical mechanisms for suppression of convection through raised lifting condensation levels have been proposed (e.g., Fasullo 2010). Second, regarding the dynamical component of change, over the SA landmass we find intermodel uncertainty to be associated with low-level circulation patterns associated with zonal gradients in SST changes in the subtropical Indian Ocean and the intensity of continental heating and the thermal low pressure center. The land–sea heating contrast has been hypothesized by Bayr and Dommenget (2013) to be a driver of enhanced convergence over land with implications for convection at the continental scale, but our results indicate that the response can be complex in this case leading to a northward shift of the ITCZ/SIOCZ and wetting–drying at the regional scale. Over both the ocean and land examination of intermodel dispersal yields structures with less zonal uniformity of change than represented by the MMM response. The sensitivity of ΔP_{Shift} across models to the pattern of SST structures and their resemblance to contemporary modes of variability suggests that further analysis of future SST

patterns and assessment of model representation of present rainfall–SST teleconnections and mean state biases may be useful to inform our interpretation of the credibility of projected changes.

This paper provides new insight of projected precipitation mechanisms of change over southern Africa by identifying the dominant pattern of change over southern Africa (the wetting–drying dipole). Drivers of this projected change are evaluated and attempts are made to quantify the associated uncertainty. Regional circulation analysis is additionally performed to shed light on the patterns driving future dynamic precipitation changes in OND and DJF, which are in agreement with previous studies over other regions (e.g., Kent et al. 2015).

Acknowledgments. This work was supported financially by the Peter Carpenter Scholarship for African Climate Change at the University of Sussex and the Future Climate for Africa (FCFA) regional consortium project UMFULA funded by NERC (Grant NE/M020258/1) and the U.K. government's Department for International Development (DfID). We also acknowledge the World Climate Research Programme's Working Group on Coupled Modelling responsible for CMIP5 model data, which was provided by the Program for Climate Model Diagnosis and Intercomparison (PCMDI). More information on this model data can be found at the PCMDI website (https://pcmdi.llnl.gov/).

REFERENCES

Ackerman, A. S., O. B. Toon, D. E. Stevens, A. J. Heymsfield, V. Ramanathan, and E. J. Welton, 2000: Reduction of tropical cloudiness by soot. *Science*, **288**, 1042–1047, https://doi.org/10.1126/science.288.5468.1042.

Allen, C. D., and Coauthors, 2010: A global overview of drought and heat-induced tree mortality reveals emerging climate change risks for forests. *For. Ecol. Manage.*, **259**, 660–684, https://doi.org/10.1016/j.foreco.2009.09.001.

Archer, E. R. M., W. A. Landman, M. A. Tadross, J. Malherbe, H. Weepener, P. Maluleke, and F. M. Marumbwa, 2017: Understanding the evolution of the 2014–2016 summer rainfall seasons in southern Africa: Key lessons. *Climate Risk Manage.*, **16**, 22–28, https://doi.org/10.1016/j.crm.2017.03.006.

Basher, R., and S. Briceño, 2006: Climate and disaster risk reduction in Africa. *Climate Change and Africa*, P. S. Low, Ed., Cambridge University Press, 271–286.

Baudoin, M. A., C. Vogel, K. Nortje, and M. Naik, 2017: Living with drought in South Africa: Lessons learnt from the recent El Niño drought period. *Int. J. Disaster Risk Reduct.*, **23**, 128–137, https://doi.org/10.1016/j.ijdrr.2017.05.005.

Bayr, T., and D. Dommenget, 2013: The tropospheric land–sea warming contrast as the driver of tropical sea level pressure changes. *J. Climate*, **26**, 1387–1402, https://doi.org/10.1175/JCLI-D-11-00731.1.

Behera, S. K., and T. Yamagata, 2001: Subtropical SST dipole events in the southern Indian Ocean. *Geophys. Res. Lett.*, **28**, 327–330, https://doi.org/10.1029/2000GL011451.

Bony, S., G. Bellon, D. Klocke, S. Sherwood, S. Fermepin, and S. Denvil, 2013: Robust direct effect of carbon dioxide on tropical circulation and regional precipitation. *Nat. Geosci.*, **6**, 447–451, https://doi.org/10.1038/ngeo1799.

Byrne, M. P., and P. A. O'Gorman, 2013: Link between land–ocean warming contrast and surface relative humidities in simulations with coupled climate models. *Geophys. Res. Lett.*, **40**, 5223–5227, https://doi.org/10.1002/grl.50971.

Chadwick, R., 2016: Which aspects of CO_2 forcing and SST warming cause most uncertainty in projections of tropical rainfall change over land and ocean? *J. Climate*, **29**, 2493–2509, https://doi.org/10.1175/JCLI-D-15-0777.1.

——, I. Boutle, and G. Martin, 2013: Spatial patterns of precipitation change in CMIP5: Why the rich do not get richer in the tropics. *J. Climate*, **26**, 3803–3822, https://doi.org/10.1175/JCLI-D-12-00543.1.

Chou, C., and J. D. Neelin, 2004: Mechanisms of global warming impacts on regional tropical precipitation. *J. Climate*, **17**, 2688–2701, https://doi.org/10.1175/1520-0442(2004)017<2688:MOGWIO>2.0.CO;2.

——, ——, C. A. Chen, and J. Y. Tu, 2009: Evaluating the "rich-get-richer" mechanism in tropical precipitation change under global warming. *J. Climate*, **22**, 1982–2005, https://doi.org/10.1175/2008JCLI2471.1.

Christensen, J. H., and Coauthors, 2013: Climate phenomena and their relevance for future regional climate change. *Climate Change 2013: The Physical Science Basis*, T. F. Stocker et al., Eds., Cambridge University Press, 1217–1308.

Collins, M., R. E. Chandler, P. M. Cox, J. M. Huthnance, J. Rougier, and D. B. Stephenson, 2012: Quantifying future climate change. *Nat. Climate Change*, **2**, 403–409, https://doi.org/10.1038/nclimate1414.

Cook, C., C. J. C. Reason, and B. C. Hewitson, 2004: Wet and dry spells within particularly wet and dry summers in the South African summer rainfall region. *Climate Res.*, **26**, 17–31, https://doi.org/10.3354/cr026017.

Cook, K. H., 2000: The south Indian convergence zone and interannual rainfall variability over southern Africa. *J. Climate*, **13**, 3789–3804, https://doi.org/10.1175/1520-0442(2000)013<3789:TSICZA>2.0.CO;2.

——, 2001: A Southern Hemisphere wave response to ENSO with implications for southern Africa precipitation. *J. Atmos. Sci.*, **58**, 2146–2162, https://doi.org/10.1175/1520-0469(2001)058<2146:ASHWRT>2.0.CO;2.

Dessai, S., M. Hulme, R. Lempert, and R. Pielke, 2009: Do we need better predictions to adapt to a changing climate? *Eos, Trans. Amer. Geophys. Union*, **90**, 111–112, https://doi.org/10.1029/2009EO130003.

DiNezio, P. N., G. A. Vecchi, and A. C. Clement, 2013: Detectability of changes in the walker circulation in response to global warming. *J. Climate*, **26**, 4038–4048, https://doi.org/10.1175/JCLI-D-12-00531.1.

Dong, B., J. M. Gregory, and R. T. Sutton, 2009: Understanding land–sea warming contrast in response to increasing greenhouse gases. Part I: Transient adjustment. *J. Climate*, **22**, 3079–3097, https://doi.org/10.1175/2009JCLI2652.1.

Emori, S., and S. J. Brown, 2005: Dynamic and thermodynamic changes in mean and extreme precipitation under changed climate. *Geophys. Res. Lett.*, **32**, L17706, https://doi.org/10.1029/2005GL023272.

Fasullo, J. T., 2010: Robust land–ocean contrasts in energy and water cycle feedbacks. *J. Climate*, **23**, 4677–4693, https://doi.org/10.1175/2010JCLI3451.1.

Flato, G., and Coauthors, 2013: Evaluation of climate models. *Climate Change 2013: The Physical Science Basis*, T. F. Stocker et al., Eds., Cambridge University Press, 741–866, https://doi.org/10.1017/CBO9781107415324.020.

Goddard, L., and N. E. Graham, 1999: Importance of the Indian Ocean for simulating rainfall anomalies over eastern and southern Africa. *J. Geophys. Res.*, **104**, 19 099–19 116, https://doi.org/10.1029/1999JD900326.

Hackenbruch, J., T. Kunz-Plapp, S. Müller, and J. W. Schipper, 2017: Tailoring climate parameters to information needs for local adaptation to climate change. *Climate*, **5**, 25, https://doi.org/10.3390/cli5020025.

Hallegatte, S., A. Shah, C. Brown, R. Lempert, and S. Gill, 2012: Investment decision making under deep uncertainty—Application to climate change. World Bank Policy Research Working Paper 6193, 39 pp.

Hansen, J., M. Sato, and R. Ruedy, 1997: Radiative forcing and climate response. *J. Geophys. Res.*, **102**, 6831–6864, https://doi.org/10.1029/96JD03436.

Held, I. M., and B. J. Soden, 2000: Water vapor feedback and global warming. *Ann. Rev. Energy Environ.*, **25**, 441–475, https://doi.org/10.1146/annurev.energy.25.1.441.

—— and ——, 2006: Robust responses of the hydrological cycle to global warming. *J. Climate*, **19**, 5686–5699, https://doi.org/10.1175/JCLI3990.1.

Huang, P., S.-P. Xie, K. Hu, G. Huang, and R. Huang, 2013: Patterns of the seasonal response of tropical rainfall to global warming. *Nat. Geosci.*, **6**, 357–361, https://doi.org/10.1038/ngeo1792.

Huang, Y., W. L. Chameides, and R. E. Dickinson, 2007: Direct and indirect effects of anthropogenic aerosols on regional precipitation over East Asia. *J. Geophys. Res.*, **112**, D03212, https://doi.org/10.1029/2006JD007114.

IPCC, 2007: *Climate Change 2007: The Physical Science Basis.* S. Solomon et al., Eds., Cambridge University Press, 996 pp.

——, 2013: *Climate Change 2013: The Physical Science Basis.* T. F. Stocker et al., Eds., Cambridge University Press, 1535 pp, https://doi.org/10.1017/CBO9781107415324.

Kent, C., R. Chadwick, and D. P. Rowell, 2015: Understanding uncertainties in future projections of seasonal tropical precipitation. *J. Climate*, **28**, 4390–4413, https://doi.org/10.1175/JCLI-D-14-00613.1.

Knutti, R., and J. Sedláček, 2013: Robustness and uncertainties in the new CMIP5 climate model projections. *Nat. Climate Change*, **3**, 369–373, https://doi.org/10.1038/nclimate1716.

——, R. Furrer, C. Tebaldi, J. Cermak, and G. A. Meehl, 2010: Challenges in combining projections from multiple climate models. *J. Climate*, **23**, 2739–2758, https://doi.org/10.1175/2009JCLI3361.1.

Kusangaya, S., M. L. Warburton, E. A. van Garderen, and G. P. Jewitt, 2014: Impacts of climate change on water resources in southern Africa: A review. *Phys. Chem. Earth*, **67**, 47–54, https://doi.org/10.1016/j.pce.2013.09.014.

Lazenby, M. J., M. C. Todd, and Y. Wang, 2016: Climate model simulation of the South Indian Ocean Convergence Zone: Mean state and variability. *Climate Res.*, **68**, 59–71, https://doi.org/10.3354/cr01382.

Lempert, R. J., and M. T. Collins, 2007: Managing the risk of uncertain threshold responses: Comparison of robust, optimum, and precautionary approaches. *Risk Anal.*, **27**, 1009–1026, https://doi.org/10.1111/j.1539-6924.2007.00940.x.

Lohmann, U., and J. Feichter, 2005: Global indirect aerosol effects: A review. *Atmos. Chem. Phys.*, **5**, 715–737, https://doi.org/10.5194/acp-5-715-2005.

Ma, J., and S.-P. Xie, 2013: Regional patterns of sea surface temperature change: A source of uncertainty in future projections of precipitation and atmospheric circulation. *J. Climate*, **26**, 2482–2501, https://doi.org/10.1175/JCLI-D-12-00283.1.

——, ——, and Y. Kosaka, 2012: Mechanisms for tropical tropospheric circulation change in response to global warming. *J. Climate*, **25**, 2979–2994, https://doi.org/10.1175/JCLI-D-11-00048.1.

Manhique, A. J., C. J. C. Reason, L. Rydberg, and N. Fauchereau, 2011: ENSO and Indian Ocean sea surface temperatures and their relationships with tropical temperate troughs over Mozambique and the southwest Indian Ocean. *Int. J. Climatol.*, **31**, 1–13, https://doi.org/10.1002/joc.2050.

McSweeney, C. F., and R. G. Jones, 2013: No consensus on consensus: The challenge of finding a universal approach to measuring and mapping ensemble consistency in GCM projections. *Climatic Change*, **119**, 617–629, https://doi.org/10.1007/s10584-013-0781-9.

Meadows, M. E., 2006: Global change and southern Africa. *Geogr. Res.*, **44**, 135–145, https://doi.org/10.1111/j.1745-5871.2006.00375.x.

Meehl, G. A., and Coauthors, 2007: Global climate projections. *Climate Change 2007: The Physical Science Basis*, S. Solomon et al., Eds., Cambridge University Press, 747–845.

Munday, C., and R. Washington, 2017: Circulation controls on southern African precipitation in coupled models: The role of the Angola low. *J. Geophys. Res. Atmos.*, **122**, 861–877, https://doi.org/10.1002/2016JD025736.

Neelin, J. D., C. Chou, and H. Su, 2003: Tropical drought regions in global warming and El Niño teleconnections. *Geophys. Res. Lett.*, **30**, 2275, https://doi.org/10.1029/2003GL018625.

Niang, I., O. C. Ruppel, M. A. Adrabo, A. Essel, C. Lennard, J. Padgham, and P. Urquhart, 2014: Africa. *Climate Change 2014: Impacts, Adaptation, and Vulnerability. Part B: Regional Aspects.* V. R. Barros et al., Eds., Cambridge University Press, 1199–1265.

Pitman, A. J., 2003: The evolution of, and revolution in, land surface schemes designed for climate models. *Int. J. Climatol.*, **23**, 479–510, https://doi.org/10.1002/joc.893.

Ratnam, J. V., S. K. Behera, Y. Masumoto, and T. Yamagata, 2014: Remote effects of El Niño and Modoki events on the austral summer precipitation of southern Africa. *J. Climate*, **27**, 3802–3815, https://doi.org/10.1175/JCLI-D-13-00431.1.

Reason, C. J. C., 2001: Subtropical Indian Ocean SST dipole events and southern African rainfall. *Geophys. Res. Lett.*, **28**, 2225–2227, https://doi.org/10.1029/2000GL012735.

——, W. Landman, and W. Tennant, 2006: Seasonal to decadal prediction of southern African climate and its links with variability of the Atlantic Ocean. *Bull. Amer. Meteor. Soc.*, **87**, 941–955, https://doi.org/10.1175/BAMS-87-7-941.

Rowell, D. P., 2012: Sources of uncertainty in future changes in local precipitation. *Climate Dyn.*, **39**, 1929–1950, https://doi.org/10.1007/s00382-011-1210-2.

——, 2013: Simulating SST teleconnections to Africa: What is the state of the art? *J. Climate*, **26**, 5397–5418, https://doi.org/10.1175/JCLI-D-12-00761.1.

——, B. B. Booth, S. E. Nicholson, and P. Good, 2015: Reconciling past and future rainfall trends over East Africa. *J. Climate*, **28**, 9768–9788, https://doi.org/10.1175/JCLI-D-15-0140.1.

Saji, N. H., B. N. Goswami, P. N. Vinayachandran, and T. Yamagata, 1999: A dipole mode in the tropical Indian Ocean. *Nature*, **401**, 360–363, https://doi.org/10.1038/43854.

Seager, R., N. Naik, and G. A. Vecchi, 2010: Thermodynamic and dynamic mechanisms for large-scale changes in the hydrological

cycle in response to global warming. *J. Climate*, **23**, 4651–4668, https://doi.org/10.1175/2010JCLI3655.1.

Shepherd, T. G., 2014: Atmospheric circulation as a source of uncertainty in climate change projections. *Nat. Geosci.*, **7**, 703–708, https://doi.org/10.1038/ngeo2253.

Shongwe, M. E., G. J. van Oldenborgh, B. van den Hurk, B. de Boer, C. Coelho, and M. van Aalst, 2009: Projected changes in mean and extreme precipitation in Africa under global warming. Part I: Southern Africa. *J. Climate*, **22**, 3819–3837, https://doi.org/10.1175/2009JCLI2317.1.

——, ——, ——, and M. van Aalst, 2011: Projected changes in mean and extreme precipitation in Africa under global warming. Part II: East Africa. *J. Climate*, **24**, 3718–3733, https://doi.org/10.1175/2010JCLI2883.1.

Soden, B. J., and I. M. Held, 2006: An assessment of climate feedbacks in coupled ocean–atmosphere models. *J. Climate*, **19**, 3354–3360, https://doi.org/10.1175/JCLI3799.1.

Taylor, K. E., R. J. Stouffer, and G. A. Meehl, 2012: An overview of CMIP5 and the experiment design. *Bull. Amer. Meteor. Soc.*, **93**, 485–498, https://doi.org/10.1175/BAMS-D-11-00094.1.

Vecchi, G. A., B. J. Soden, A. Wittenberg, I. Held, A. Leetmaa, and M. Harrison, 2006: Weakening of tropical Pacific atmospheric circulation due to anthropogenic forcing. *Nature*, **441**, 73–76, https://doi.org/10.1038/nature04744.

Widlansky, M. J., A. Timmermann, K. Stein, S. McGregor, N. Schneider, M. England, M. Lengaigne, and W. Cai, 2013: Changes in South Pacific rainfall bands in a warming climate. *Nat. Climate Change*, **3**, 417–423, https://doi.org/10.1038/nclimate1726.

Xie, S.-P., C. Deser, G. A. Vecchi, J. Ma, H. Teng, and A. T. Wittenberg, 2010: Global warming pattern formation: Sea surface temperature and rainfall. *J. Climate*, **23**, 966–986, https://doi.org/10.1175/2009JCLI3329.1.